

# Practical evaluation of carrier sensing for a LoRa wildlife monitoring network

Morgan O’Kennedy<sup>1</sup>, Thomas Niesler<sup>2</sup>, Riaan Wolhuter<sup>2</sup>, Nathalie Mitton<sup>3</sup>

<sup>1,2</sup> Dept. of Electrical and Electronic Engineering

<sup>1,2</sup> University of Stellenbosch, Stellenbosch, South Africa, <sup>3</sup>Inria, Lille, France

<sup>1</sup>morgan.okennedy@gmail.com, <sup>2</sup>{trn, wolhuter}@sun.ac.za, <sup>3</sup>nathalie.mitton@inria.fr

**Abstract**— We consider the technique of carrier sensing for application in a LoRa mesh network aimed at wildlife monitoring. A key challenge in this application is to limit collisions in order to increase the channel capacity. Since CSMA is very rarely applied in LoRa-based networks, our goal is to determine its practical viability. We evaluate the LoRa Channel Activity Detection (CAD) mechanism under laboratory and field conditions. Our results show that both preamble and payload symbols are detectable even at distances exceeding 4 km. Detecting LoRa preamble symbols had a SNR advantage of between 1 and 2 dB over payload symbols. Furthermore, we find that by taking at least 8 consecutive CAD measurements, a clear channel assessment (CCA) comparable to the LoRa frame reception rate can be achieved between two nodes.

**Keywords**—LoRa, CSMA, mesh network, wireless sensor networks, LPWAN

## I. INTRODUCTION

With the rapid decrease in the populations of threatened animal species, the ability to remotely monitor wildlife in their natural habitat has become an important necessity. In South Africa, the population of rhinoceros is under severe threat due to illegal poaching for their horns. Over the period 2013 – 2018, approximately 1000 rhinos were killed each year in national parks by poachers [2]. These parks are in remote locations, often with poor infrastructure and no cellular network coverage. They often cover large areas, with the largest, the Kruger National Park, covering more than 20 000 square kilometers. Consequently, current anti-poaching strategies have proved to be largely ineffective.

We have developed prototype animal-borne biotelemetry sensor tags with the aim of detecting abnormal behavioral patterns that can alert a proactive response [1]. A major challenge remains the reliable gathering of data in a cost-effective manner over the vast, remote areas that form the habitat of the animals under threat. In [3] the authors have evaluated several low-cost radio transceiver modules and found that LoRa-capable devices outperformed similar candidates for a practical wildlife monitoring wireless sensor network.

In a LoRa network, channel access is typically attained by a random-access method, functionally similar to ALOHA where collisions are not explicitly avoided [4, 5]. Such networks have a well-known channel capacity limitation of roughly 0.18 packets per packet-time [6, 7]. This limitation might have a significant performance impact on our intended low-cost LoRa-based mesh network (Fig. 1) for the following reasons:

1. By maximizing the communication range, the Time-On-Air (ToA) per data transmission can be several seconds long.

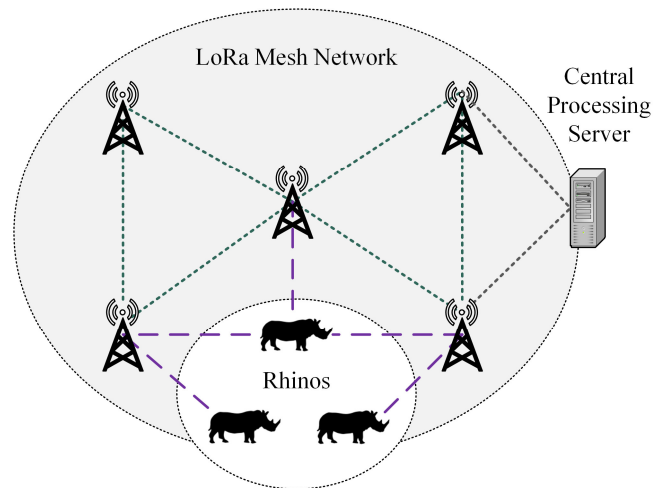


Fig. 1. A wildlife monitoring mesh network.

2. For a simplistic and low-cost implementation, a single mesh node radio module implies a network-wide default channel on which all nodes communicate.
3. The mesh nodes will further fill the channel occupancy by forwarding sensor data to a central processing server.

Several studies have analyzed the protentional benefit of Carrier-Sense Multiple Access (CSMA) for LoRa-based networks [9]-[11]. In [10], the authors have assessed a range of channel access control protocols and demonstrated by means of simulation that CSMA is scalable and the best amongst those considered in terms of reliability and energy consumption for a high node count. However, there is very little information on the practical performance of LoRa CSMA over longer distances. Therefore, in this paper, we propose a method with which to evaluate the LoRa CSMA mechanism and to determine its viability for a Medium Access Protocol (MAC) design that aims to decrease collisions and thus increase channel capacity.

In the next section, we will discuss the necessary background and related work, followed by an analysis of the LoRa carrier sensing mechanism in Section III. Our experimental setup is described in Section IV and our results presented and discussed in Section V. Finally, Section VI concludes the paper.

## II. BACKGROUND

### A. LoRa and LoRaWAN

LoRa is a proprietary spread spectrum modulation scheme, owned by the Semtech Corporation. It implements a variation of chirp spread spectrum with the capability of increased communication range in exchange for a low data

rate. The data rate for a given channel bandwidth (BW) is determined by choosing a spreading factor (SF) parameter where  $SF \in \{7, \dots, 12\}$ . The higher the SF, the more BW is used per symbol, resulting in a lower data rate and increased receiver sensitivity. The LoRa symbol period is given in [20] by:

$$T_{sym} = \frac{2^{SF}}{BW} \quad (1)$$

In addition to the precise control of the data rate, the spreading factor also allows simultaneous transmissions in a shared channel, as the receiver is able to differentiate between quasi-orthogonal signals associated with different spreading factor signals [18].

The LoRa physical frame structure has four parts: a preamble (which is used for receiver synchronization), an optional frame header (which consists of additional frame parameters), a payload and finally an optional payload CRC.

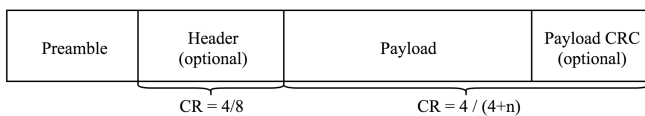


Fig. 2. The LoRa physical frame structure. The payload Coding Rate (CR) parameter has a user selectable range  $\{4/5, 4/6, 4/7, 4/8\}$  [5].

LoRaWAN is an open standard MAC protocol that utilizes LoRa modulation as the physical layer [21]. It has gained popularity in its use for a Low-Power Wide-Area Network (LPWAN) technology intended for the Internet of Things (IoT). The protocol acts as a star-topology networking protocol for managing communication between end-devices and internet gateways. The gateway is then responsible for routing packets to a central network server. Readers unfamiliar with LoRaWAN or LoRa are referred to [17] and [20] for a more comprehensive description.

### B. LoRa frequency bands and duty cycles

The most popular frequency bands used by LoRa (and especially LoRaWAN) devices are 868MHz in Europe and 915MHz in the Americas. In Europe and Southern Africa, the ETSI harmonised standards restrict transmissions by end-devices to a maximum duty cycle of 1% [23]. This accounts to a maximum ToA of 36 seconds per hour. Due to improved radio propagation, we have chosen 433MHz instead of 868MHz as the default frequency band. This band also has the additional benefit of a less restrictive duty cycle (maximum 10%), but at a cost of a slightly lower maximum transmission power. Nevertheless, even after considering the diminished power, the theoretical electromagnetic propagation is still superior at 433MHz.

### C. LoRa-based wildlife monitoring networks

Several LoRa-based wildlife monitoring projects have been presented in the literature, many with unique concepts and each with its own benefits and limitations. In [14]-[15], the authors have proposed a dual radio architecture that uses both Bluetooth Low Energy (BLE) and LoRa modules. They consider a BLE opportunistic mesh routing strategy that uses a store-carry-and-forward scheme amongst animal herds to ultimately offload concatenated data payloads to a LoRaWAN gateway. Although this reduces networking

overhead, the single-hop LoRaWAN connectivity does not provide the coverage that would be needed for poaching alerts in large African parks. Indeed, LPWAN wildlife monitoring initiatives have already been successfully deployed [8], but the targeted parks are either small or the existing infrastructure and terrain allows for single hop communication. Since it is both impractical and uneconomical to provide internet gateways in much larger parks, this study focusses on LoRa mesh nodes that do not rely on LoRaWAN.

In [16], the authors emphasize the need for a multi-hop protocol to deliver extended coverage, together with a multi-channel capability to provide capacity. They suggest a Time-Division Multiple Access (TDMA) approach in which all nodes are synchronized by means of a GPS clock and transmit during their reserved time-slots. This design shares our goal of rhino protection, giving priority to alert messages and allowing for regular monitoring updates. Although the LoRa CSMA feature is used to detect occupied time-slots, the authors do not describe provide any detail of its practical implementation. The protocol also does not consider the power implications of the required frequent GPS-time synchronization. Our animal-borne sensor tags are designed with exceptional frugality in terms of power usage in order to maximize longevity and therefore frequent GPS use is not possible. The on-board clock is insufficient to keep the tag synchronized in the long-term and a dependence on connectivity for synchronization would be unreliable. We therefore require a protocol that will allow asynchronous communication in order to support infrequent tag wake-up periods and that does not depend on accurate time synchronization for each initiated transmission.

### D. CSMA on LoRa-based networks

It has been demonstrated by simulation that CSMA can be effectively applied to LoRa networks with a high node count [9]-[11]. Unfortunately, practical verification is difficult and resource intensive. Nevertheless, a practical experiment with 50 nodes was conducted in [12] to determine the effectiveness of CSMA as a collision avoidance mechanism. This work showed a ~20% higher packet reception rate when using inter-packet delays of 2 - 5 seconds and a payload size of 8 bytes. Unfortunately, neither the experimental node distances nor the radio conditions are described.

A practical evaluation of CSMA for long LoRa payloads between 2 nodes was performed in [13]. First, a protocol was adapted from the IEEE 802.11 Distributed Coordinated Function's (DCF) basic CSMA mechanism. It was found that this mechanism becomes unreliable with increased range which impacts negatively in a real-world deployment. For example, the technique was found to be effective up to 1 km in non-line-of-sight conditions and only up to 400m in dense vegetation. An extended DCF Inter-Frame Space (DIFS) was suggested and defined as the maximum transmission ToA in which periodic carrier detection was performed. However, the distance and radio conditions for which the proposed mechanism is expected to become unreliable were not described. Finally, both [12] and [13] find that the CSMA mechanism can occasionally successfully detect the payload part of a frame. However, this is an unspecified functionality of the module [19] and no information is available on the limitations of this unexpected behaviour.

Apart from the studies mentioned above, we are not aware of other practical CSMA implementations on LoRa-

based networks. For instance, the LoRaWAN standard [21] does not apply CSMA in its design.

The next section will describe the CSMA technique used by the LoRa radio module, highlight its design limitations and illustrate how we adapted the CSMA concepts from another network type for our LoRa multi-hop MAC protocol.

### III. THE CARRIER-SENSE MULTIPLE ACCESS MECHANISM

#### A. LoRa physical CSMA capabilities

LoRa radio modules can detect channel activity using two distinct mechanisms. First, the Received Signal Strength Indicator (RSSI) can be monitored. The RSSI level is a relative measure of the total RF energy a node receives at its antenna, regardless of whether it is a LoRa signal or not. Although this approach can be suitable when the signal is strong, the LoRa module is able to demodulate transmissions that fall below the RF noise floor due to its inherent processing gain (Tab. I). Thus, for our intended long-range application, this mechanism is not ideal.

TABLE I.  
RANGE OF SPREADING FACTORS AND ASSOCIATED PERIODS AND RECEPTION SENSITIVITY [19].

Spreading Factor	Symbol period (1) at 125 kHz BW (ms)	CAD duration (symbols)	Demodulator cut-off SNR (dB)
7	1.024	2.40	- 7.5
8	2.048	2.01	-10.0
9	4.096	1.86	-12.5
10	8.192	1.83	-15.0
11	16.384	1.84	-17.5
12	32.768	1.86	-20.0

The second mechanism is the so-called “Channel Activity Detection” (CAD) and is designed specifically to detect LoRa preamble signals (chirps) below the noise floor. This function is activated by placing the radio module into a specific CAD-mode in which it captures radio samples for about one symbol period from the selected channel [19]. The modem then searches for a correlation between the captured samples and the ideal chirp waveform for the selected spreading factor (SF). If the correlation is strong, a “CAD detected” interrupt is generated. Otherwise, a “CAD done” interrupt is raised<sup>1</sup>. The result of a CAD measurement is thus a single binary value. The total duration of this operation is about 2 symbol periods (Tab. I) and during this time the receiver is not able to receive packets normally. The CAD-technique is the recommended mechanism employed by the LoRa module for a CSMA clear channel assessment (CCA) and is the focus of the remainder of this paper. A major drawback of its use is the stated inability to detect the payload part of the LoRa frame<sup>2</sup>. Currently, it is also unclear under which radio conditions the CAD measurements become unreliable. Therefore, the key aim in Section IV is to discover the limitations of the CAD mechanism more precisely to allow informed decisions in our MAC protocol design.

<sup>1</sup> Only the SX127x family of LoRa radio modules are considered here.

<sup>2</sup> The most recent SX126x radio modules claim to support CAD-detection in the physical frame payload. Due to the unavailability of such integrated modules in the 433MHz band at the time of writing, this was not evaluated.

#### B. CSMA/CA implementation in IEEE 802.11

The IEEE 802.11 DCF standard [22] is widely adopted as the MAC-layer for WLAN and wireless ad-hoc networks. It specifies a physical and virtual method for performing CSMA. The “basic mode” achieves physical carrier sensing in the following manner:

1. If a node that wishes to transmit senses the channel to be idle, it transmits only after determining the channel to be continuously idle for a DIFS duration.
2. If the channel is sensed to be busy, the node waits until the channel is sensed to be idle for a DIFS duration. The node then waits for a further random backoff period chosen from a backoff Contention Window (CW)  $\{0, \dots, CW_{\min} - 1\}$  where  $CW_{\min}$  is the initial backoff window size.
3. The backoff counter is decreased at each consecutive idle slot and maintained during each busy slot.
4. When the backoff counter reaches 0, the node transmits its packet and waits for an acknowledgement (ACK). If the ACK is received within a Short Inter-Frame Space (SIFS), the transmission was successful.
5. If an ACK is not received within an ACK timeout period, it restarts the process from 2 with the random backoff counter chosen from a backoff window size increased by a factor 2 (but not exceeding  $CW_{\max}$ ).

In order to alleviate the well-known hidden terminal problem, an optional “virtual carrier sensing” mechanism is also defined. It is usually configured to be used for frames exceeding a specified size. A request-to-send/clear-to-send (RTS/CTS) handshake is incorporated (Fig. 3) to reserve access to the channel as follows:

1. When a node wants to transmit a data frame, it first sends an RTS to the destination which contains the total time that will be required for the remaining exchange of frames.
2. When the destination receives the RTS frame, it responds with a CTS after a SIFS delay. The CTS gives the requesting node the permission to send its data and notifies other nodes in the interference area of an impending exchange.
3. Any listening node that receives the CTS for which it was not intended will update its Network Allocation Vector (NAV) with the reserved duration and will refrain from accessing the channel during this period.
4. The data transmission starts after the successful RTS/CTS exchange and is confirmed with a subsequent ACK. If the ACK is not received, the backoff procedure is initiated.

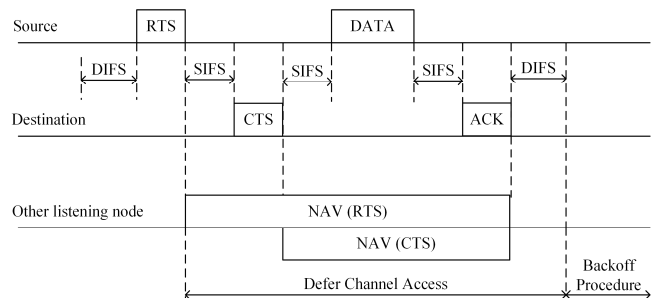


Fig. 3. The optional virtual carrier sensing mechanism defined in IEEE 802.11.

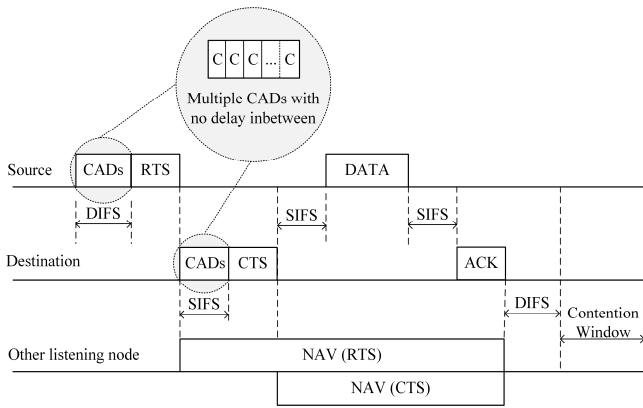


Fig. 4. A combined CSMA for a LoRa multi-hop wildlife network.

### C. A combined CSMA implementation for a LoRa multi-hop wildlife network

In the previous work discussed in Section II-D, CSMA was considered only for single-hop LoRa communication. Correspondingly, only physical carrier sensing was evaluated. Our envisioned application in a multi-hop scenario is expected to suffer from hidden terminals which negatively impact on the network's performance. Thus, we propose to combine the concepts of both the physical and virtual carrier sensing defined in IEEE 802.11 for our wildlife monitoring network. Currently, the physical carrier sensing mechanism is applied exclusively to the mesh (backhaul) nodes for two reasons. Firstly, the animal-borne tag antenna will be close to the ground, and secondly, the animal is likely to be within dense vegetation. This contrasts to the elevated and exposed placement of the mesh nodes, which will ensure favourable conditions for carrier sensing.

We therefore propose physical carrier sensing using a method similar to [13] but applied in conjunction with the RTS/CTS control frames (Fig. 4). In addition to alleviating the hidden terminal problem, the control frames can be employed to further augment the protocol. We have exploited the RTS/CTS frames for negotiating a separate data channel on which the longer data payload will be sent. This diminishes the network traffic on the default control channel, and as a result the probability of collisions. Since in our application the control frames have a maximum size of 8 bytes, both IFS durations could also be significantly reduced. However, the number of consecutive CADs required to accurately perform a CCA is currently unknown. This parameter will also determine the SIFS and DIFS durations of the CSMA implementation.

## IV. EXPERIMENTAL SETUP

### A. Node hardware configuration

We have used the Nucleo-L073RZ development board as the main processing unit for all nodes in our experiments. The Adafruit RFM96W 433MHz LoRa module was connected and configured as the radio transceiver (Tab. II). The nodes were supplied with grid power in the laboratory experiments. In the outdoors, however, power was provided by 4W solar panels and a 10Ah Li-ion battery pack.

TABLE II.  
RFM96W MODULE CONFIGURATION.

Module Parameter	Value
RF Frequency	433.175 MHz
Bandwidth	125 kHz
Preamble Symbols	8
Coding Rate	4/5
Spreading Factor	[7, 9, 11]

### B. Evaluation of CAD in the laboratory

A laboratory test was conducted to simulate the radio module's carrier sensing behaviour under poor radio conditions. The objective of this experiment was to find the precise limitations of the CAD mechanism provided by the RFM96W. This information will provide the insight needed to design a protocol that is able to perform an accurate CCA.

We made use of two RF step attenuators to accurately control the RF power ( $-121 - 0$  dB) transmitted from a master node to several receiver nodes. Before starting the measurements, the master node transmission was attenuated to the threshold at which the receiver could still successfully decode the frame. The receiver nodes were placed inside a RF shielded enclosure to ensure that no spurious emissions would influence the measurements. The attenuated master node signal was then fed to an antenna inside the enclosure (Fig. 5). The following CAD measurement procedure was then performed for SFs 7, 9 and 11:

- The master would set its RF power to maximum  $P_{\max}$ . It then sends a notification to all listening nodes informing them that a CAD measurement transmission is about to begin.
- When a node receives the notification, it waits for a SIFS duration after which it performs 20 consecutive CAD measurements. The master node is configured to start another 8-byte transmission containing random data at exactly the same time as the first measurement.
- The listening node saves the result of each CAD measurement, together with the RSSI and SNR of the measurement notification. These results are sent back to the master node at coordinated intervals.
- The master node then reduces its transmission power by 1 dBm and the process repeats until  $P_{\min}$ . The transmission power is then restored to  $P_{\max}$  and the full process is repeated.

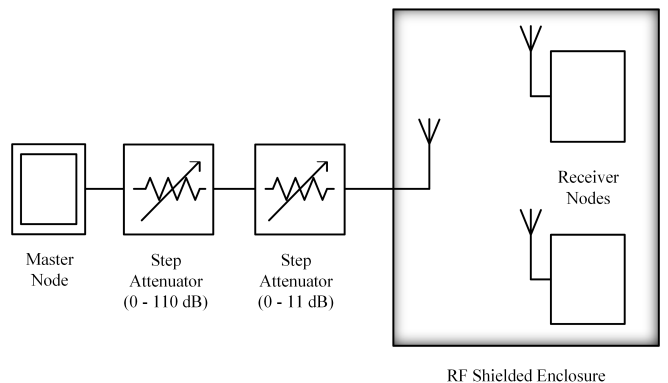


Fig. 5. The laboratory setup for evaluation of the CAD mechanism.

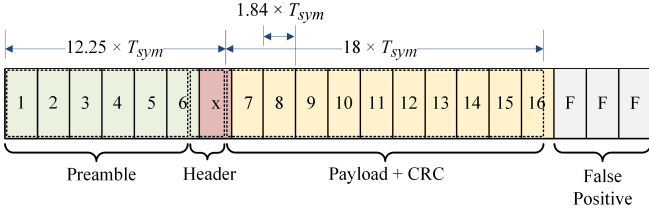


Fig. 6. The structure of the 20 consecutive CAD measurements, showing the near-perfect synchronization for a 8-byte payload at SF11. A total of 16 successful detections can be performed.

With no RF attenuation, the CAD measurements were observed to always successfully detect the full 8-byte physical frame sent by the master, with the exception of the measurement during the frame header (Fig. 6). This measurement could never detect the channel as occupied and was consequently discarded in the calculation of the CAD error rates. The preamble and payload consist of 6 and 10 measurements respectively, except in the case for SF7, where the preamble consists of 5 measurements. Three additional measurements after the completion of the transmission were used for calculating the CAD false positive rate. Attenuated transmissions resulted in a lower probability of successful CADs during both parts of the frame. To gain reliable averages, the experiment was repeated to obtain about 35 000 frame measurements for each SF. A second experiment considered only CAD within the payload part of the physical frame. This was achieved by including appropriate delays between transmitter and receiver. It was observed that the results correspond with simply discarding all preamble measurements from the first experiment. The complete experimental results will be presented in Section V.

### C. Evaluation of CAD in the outdoors

To validate our laboratory measurement results in a real-world environment, we performed the same procedure described in the previous section in an outdoor environment. A master node was installed on the roof of the Department's building at an estimated height of 22m above ground level. Secondary field nodes were placed on farmlands approximately 4 km away (Fig. 7, 8). This scenario is comparable to the envisioned deployment of a sink node in a national park rest camp and a mesh node on a nearby hill. Since the CAD measurement results are sent back to the master node, they can be easily collected and analysed. The procedure was run over multiple days to capture 60 000 measurements per node.

## V. EXPERIMENTAL RESULTS

### A. Results of the laboratory experiments

The CAD error rates versus SNR at 3 different SFs are shown in Figure 9. The SNR shown is the value reported by the LoRa radio module as described in Section IV-B. For each SF dataset, all CAD measurements were grouped by SNR. CADs measured during the frame preamble and payload are calculated separately. The average CAD error rate (CER) was calculated per SNR group, given by:

$$\text{CER}_{snr} = 1 - \frac{1}{n \cdot m} \sum_{i=1}^m \sum_{j=1}^n \text{CAD}_{i,j,snr} \quad (2)$$

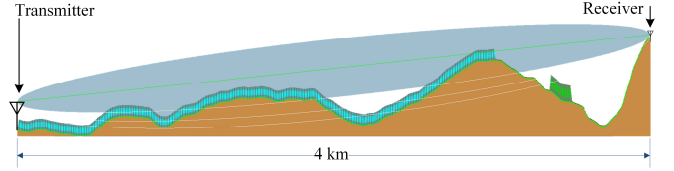


Fig. 7. The elevation profile and first Fresnel zone of a 4 km long communication link for one of our outdoor measurement.



Fig. 8. A photograph showing one of the LoRa field nodes used in our outdoor experimental evaluation.

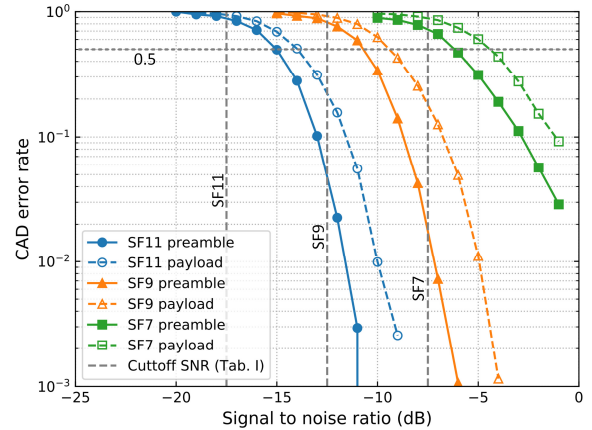


Fig. 9. Laboratory-measured CAD error rates (CER) for measurements at SF7, SF9 and SF11.

where  $m$  is the total number of CAD measurements for a particular SNR and  $n$  the number of preamble or payload measurements per frame (as shown in Fig. 6). The CER considers only the failure to detect the channel activity (false negatives). The CAD false positive rate, i.e. the detection of activity when no transmission was underway, was always measured as below  $1 \times 10^{-4}$  and is consequently not shown. The cut-off SNR associated with each spreading factor (Tab. I) is shown in grey.

It is observed that the CER plots resemble bit error rate (BER) curves. At a preamble CER of 0.5, the corresponding SNR is found to be at 1.5, 1.75 and 2.5 dB above the cut-off SNR for SF7, SF9 and SF11 respectively. Contrary to the indications in the manufacturer's official datasheet, the LoRa module was found to be able to detect channel activity during the payload part of the frame, but at a 1 – 2 dB reduced SNR sensitivity relative to the preamble.

To compensate for this reduced sensitivity during the payload, we considered the effect of performing multiple

consecutive CADs as suggested in Section III. The accumulative result from these multiple CADs is defined as the CCA. For each frame, the logical OR of  $n$  collected measurements was determined. Because of the binary nature of these values, this operation can be expressed as  $\max(\text{CAD}_1, \text{CAD}_2, \dots, \text{CAD}_n)$  so that the average CCA error rate (CCER) is defined as:

$$\text{CCER}_{snr} = 1 - \frac{1}{m} \sum_{i=1}^m \max_{j=1, \dots, n} (\text{CAD}_{j,i,snr}) \quad (3)$$

For the purpose of comparison, a theoretical estimate of the LoRa bit error probability ( $P_b$ ) was required. Several such estimates have been presented in the literature, but the one derived in [24] was found to coincide most closely with our preliminary test observations. Equation (4) was derived using a simplified decoder implementation under an additive white Gaussian noise (AWGN) channel. Assuming no forward error correction, the symbol error probability ( $P_s$ ) and frame error probability ( $P_f$ ) are given by Equations (5) and (6),

$$P_b = Q\left(\frac{\log_{12}(\text{SF})}{\sqrt{2}} \cdot \frac{E_b}{N_0}\right) \quad (4)$$

$$P_s = 1 - (1 - P_b)^{\text{SF}} \quad (5)$$

$$P_f = 1 - (1 - P_s)^n \quad (6)$$

where  $Q(x)$  is the Q-function,  $E_b/N_0$  is the energy per bit to noise spectral density ratio and  $n$  is the number of payload symbols per frame, e.g.  $n = 18$  for an 8-byte payload at SF11.

Figure 10 shows the SF11 CCER when including the entire preamble as well as when  $n \in \{1, 2, 4, 6, 8\}$  for payload measurements. The frame error probability computed using Equation (6) is shown for comparison (in grey). As might be expected, the lowest CCA is obtained when the entire preamble is consecutively measured (in black). However, it is also observed that, for 8 payload CAD measurements (in red), the CCA reliability is almost as good as measuring the entire preamble. Using fewer CADs results in a sensitivity up to 4 dB below this achievable rate. Fig. 10 also shows that, by applying 8 CADs, the CCA sensitivity is comparable to the probability of frame errors predicted by Equation (6).

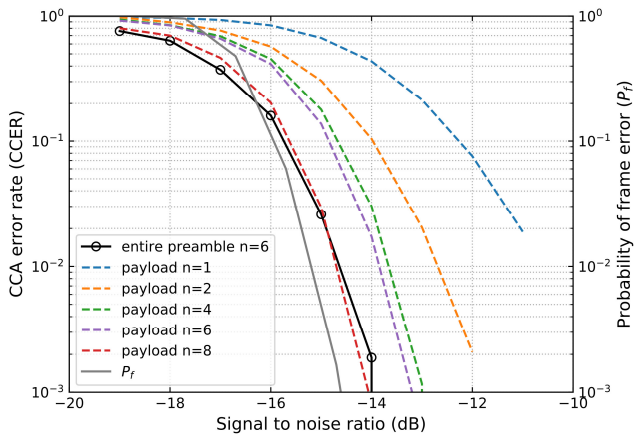


Fig. 10. Laboratory-measured CCA error rates (CCER) when using the entire preamble as well as when taking  $n$  payload measurements, all at SF11.

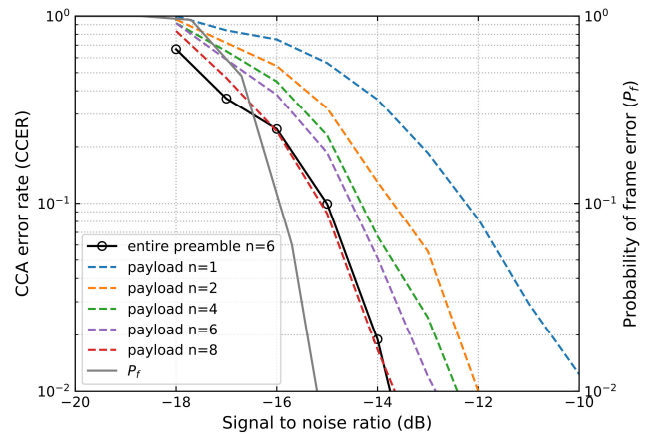


Fig. 11. Outdoor-measured CCA error rates (CCER) when using the entire preamble as well as when taking  $n$  payload measurements at SF11.

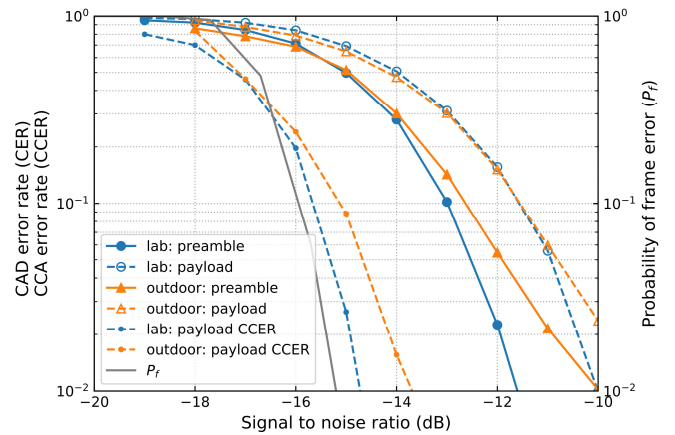


Fig. 12. Comparison of outdoor and laboratory CAD measurements at SF11. Each CCA error rate (CCER) consists of 10 CADs measured during the payload.

### B. Results of the outdoor experiments

Figure 11 shows the CCER for the entire preamble and  $n$  payload measurements, as in Figure 10, but for the outdoor dataset. The CCER has a slightly wider deviation from the frame error probability compared to the laboratory measurements. However, our finding that 8 payload CADs are needed to achieve a CCA accuracy comparable to what can be achieved when measuring the entire preamble still holds. Consequently, to minimize the probability of detecting a false clear channel, a reliable MAC protocol should incorporate at least 8 consecutive CAD measurements for its CCA.

Figure 12 compares laboratory and outdoor experimental results for one field node. Similar results were obtained for the other field nodes. We observe a good agreement between the indoor and outdoor results for CAD error rates above  $10^{-1}$ . This indicates that the mechanism is viable even over the extended range of 4 km. The deviation observed at lower error rates was found to be due to noise introduced by the solar charger circuitry. It is also expected that interference from other LoRa nodes with a similar selected spreading factor and channel will further reduce the CCA reliability.

## VI. CONCLUSION

We have evaluated the LoRa CAD technique in order to determine its viability as a physical CSMA mechanism for a wildlife monitoring network. Indoor and outdoor experimental evaluation established that it is feasible to detect both the preamble and the payload part of the LoRa physical frame using LoRa CAD, even at distances exceeding 4 km. Applying CAD to the LoRa preamble symbols had an average SNR advantage of between 1 and 2 dB over its application to payload symbols. We also conclude that by taking 8 or more consecutive CAD measurements, a CCA sensitivity comparable to the LoRa frame reception rate can be achieved. With the additional interference from messages using the same spreading factor in a dense LoRa network, it is expected that even more CAD measurements could be required to maintain this reliability. The development of a complete MAC protocol to incorporate this mechanism is part of our ongoing work.

## ACKNOWLEDGMENT

The financial support of TIA and Telkom South Africa towards this research is gratefully acknowledged. We would also like to thank Jonathan Wotherspoon for his contribution to the development of the outdoor node infrastructure.

## REFERENCES

- [1] S. P. le Roux, R. Wolhuter, N. Stevens and T. Niesler, "Reduced Energy and Memory Requirements by On-Board Behavior Classification for Animal-Borne Sensor Applications," in *IEEE Sensors Journal*, vol. 18, no. 10, pp. 4261-4268, 2018.
- [2] Save the Rhino International, "Poaching Statistics". Accessed: Nov. 29, 2019. [Online]. Available: <https://www.savetherhino.org/>
- [3] J. Wotherspoon, R. Wolhuter and T. Niesler, "Choosing an integrated radio-frequency module for a wildlife monitoring wireless sensor network," 2017 IEEE AFRICON, Cape Town, pp. 314-319, 2017.
- [4] N. Abramson, "The Aloha System: Final Technical Report," Hawaii University: Honolulu, HI, USA, 1974.
- [5] A. Augustin, J. Yi, T. Clausen, and W. M. Townsley, "A Study of LoRa: Long Range & Low Power Networks for the Internet of Things," *Sensors*, vol. 16, no. 9, Sept. 2016. [Online]. Available: <http://www.mdpi.com/1424-8220/16/9/1466>
- [6] D. Magrin, M. Centenaro and L. Vangelista, "Performance evaluation of LoRa networks in a smart city scenario," 2017 IEEE International Conference on Communications (ICC), Paris, pp. 1-7, 2017.
- [7] F. Adelantado, X. Vilajosana, P. Tuset-Peiro, B. Martinez, J. Melia-Segui and T. Watteyne, "Understanding the Limits of LoRaWAN," in *IEEE Communications Magazine*, vol. 55, no. 9, pp. 34-40, Sept. 2017.
- [8] Kerlink, "First black rhinos protected by sensor-implants in horns," Sept. 2017. [Online]. Available: <http://www.kerlink.com/wp-content/uploads/2017/10/Kerlink.pdf>
- [9] T. To and A. Duda, "Simulation of LoRa in NS-3: Improving LoRa Performance with CSMA," 2018 IEEE International Conference on Communications (ICC), Kansas City, MO, pp. 1-7, 2018.
- [10] M. O. Farooq and D. Pesch, "A Search into a Suitable Channel Access Control Protocol for LoRa-Based Networks," 2018 IEEE 43rd Conference on Local Computer Networks (LCN), Chicago, IL, USA, pp. 283-286, 2018.
- [11] S. Ahsan, S. A. Hassan, A. Adeel and H. K. Qureshi, "Improving Channel Utilization of LoRaWAN by using Novel Channel Access Mechanism," 2019 15th International Wireless Communications & Mobile Computing Conference (IWCMC), Tangier, Morocco, pp. 1656-1661, 2019.
- [12] J. C. Liando, A. Gamage, A. W. Tengourtius, and M. Li, "Known and unknown facts of LoRa: Experiences from a large-scale measurement study," *ACM Transactions on Sensor Networks (TOSN)*, vol. 15, no. 2, p. 16, 2019.
- [13] C. Pham, "Investigating and experimenting CSMA channel access mechanisms for LoRa IoT networks," 2018 IEEE Wireless Communications and Networking Conference (WCNC), Barcelona, pp. 1-6, 2018.
- [14] E. D. Ayele, N. Meratnia and P. J. M. Havinga, "Towards a New Opportunistic IoT Network Architecture for Wildlife Monitoring System," 2018 9th IFIP International Conference on New Technologies, Mobility and Security (NTMS), Paris, pp. 1-5, 2018.
- [15] E. D. Ayele, N. Meratnia and P. J. M. Havinga, "MANER: Managed Data Dissemination Scheme for LoRa IoT Enabled Wildlife Monitoring System (WMS)," 2018 9th IFIP International Conference on New Technologies, Mobility and Security (NTMS), Paris, pp. 1-7, 2018.
- [16] V. Toldov, L. Clavier and N. Mitton, "Multi-channel Distributed MAC protocol for WSN-based wildlife monitoring," 2018 14th International Conference on Wireless and Mobile Computing, Networking and Communications (WiMob), Limassol, pp. 1-8, 2018.
- [17] J. Haxhibeqiri, E. De Poorter, I. Moerman, and J. Hoebeke, "A Survey of LoRaWAN for IoT: From Technology to Application," *Sensors*, vol. 18, no. 11, p. 3995, Nov. 2018.
- [18] D. Croce, M. Gucciardo, S. Mangione, G. Santaromita and I. Tinnirello, "Impact of LoRa Imperfect Orthogonality: Analysis of Link-Level Performance," in *IEEE Communications Letters*, vol. 22, no. 4, pp. 796-799, April 2018.
- [19] Hope RF Microelectronics, "RFM95/96/97/98(W) - Low Power Long Range Transceiver Module," v1.0; Hope RF Microelectronics: Shenzhen, China, 2016.
- [20] Semtech Corporation. "LoRa Modulation Basics - Application Note 1200.22," Revision 2, Semtech Corporation: Camarillo, CA, USA, 2015.
- [21] LoRa Alliance, "LoRaWAN 1.1 Specification," LoRa Alliance: Beaverton, OR, USA, 2017.
- [22] IEEE Standards Association, "Part 11: Wireless LAN Medium Access Control (MAC) and Physical Layer (PHY) Specifications," IEEE Std 802.11-2012, IEEE: New York, NY, USA, 2012.
- [23] ETSI, "Short Range Devices (SRD) operating in the frequency range 25 MHz to 1 000 MHz; Part 2: Harmonised Standard for access to radio spectrum for non specific radio equipment," ETSI EN 300 220-2 V3.2.1, ETSI: Sophia Antipolis, France, 2018.
- [24] B. Reynders, W. Meert and S. Pollin, "Range and coexistence analysis of long range unlicensed communication," 2016 23rd International Conference on Telecommunications (ICT), Thessaloniki, pp. 1-6, 2016.
- [25] B. Reynders and S. Pollin, "Chirp spread spectrum as a modulation technique for long range communication," 2016 Symposium on Communications and Vehicular Technologies (SCVT), Mons, pp. 1-5, 2016.